Effects of Phase Change Materials on Heat Flows Through Double Skin Façades

Thomas Wüest [1*], Lars O. Grobe [2], Andreas Luible [2]

* Corresponding author
1 Lucerne University of Applied Sciences and Arts, Institute of Civil Engineering IBI, Switzerland, thomas.wueest@hslu.ch
2 Lucerne University of Applied Sciences and Arts, Institute of Civil Engineering IBI, Switzerland

Abstract

The potential of exemplary organic and inorganic Phase Change Materials (PCMs) as façade integrated storage is tested. The impact of two PCMs on heat flows is assessed in comparison with water and concrete. The simulation-study employs a transient Modelica simulation model of a test cell featuring the Solar Energy Balanced Façade (SEBF). It is shown that, when compared to water, PCMs of identical volume change the seasonal energy balance in winter and summer by only ± 4%. Other than water, the PCMs maintain this effect even if the storage volume decreases. Due to spatial constraints, this can support the integration of thermal storage in façade design considerably. Preliminary results indicate that designing thermal storage in façades with PCMs must not only consider the latent heat storage capacity, but also take into account the combined effects of latent heat capacity, melting point, conductivity, and dead load. The application of PCMs promises to foster the integration of the technology of SEBF into façades, but the necessary deliberate selection of, and design with, PCMs requires further research.

Keywords

thermal storage, passive solar façade, trombe wall, phase change materials, solar energy balanced façade

10.7480/jfde.2021.1.5408

1 INTRODUCTION

Façades greatly affect energy demand and the level of comfort that can be achieved in a building. Both targets are addressed by a novel hybrid façade system, that integrates a controlled solar-thermal collector and storage into the transparent and opaque zones of double-skin-façades (DSF). The adaptive seasonal and daily management of solar gains of the Solar Energy Balanced Façade (SEBF) (Wüest & Luible, 2018) improves the energy balance through the passive use of solar energy. The SEBF reduces the transparent façade area, and instead introduces an opaque parapet which functions as thermal storage and mitigates daily energy flux variations. The second skin structure protects shading devices that are essential for the efficient and reliable management of solar gains absorbed by the thermal absorber, and admitted through the transparent areas.

The SEBF employs the functional principles of the Trombe Wall (TW) (Hu, He, Ji, & Zhang, 2017). TWs are passive solar façade systems, which store and redistribute heat. A typical TW combines a solid wall, acting as thermal storage, with external glazing to exploit the greenhouse effect to form a solar collector. Openings, often equipped with fans, allow for an air exchange between the attached space and the cavity of the TW. Several studies suggest that TWs have a high potential to reduce energy demand in buildings, e.g. by 50% (Quesada, Rousse, Dutil, Badache, & Hallé, 2012) and up to 69.7% (Zhang et al., 2020). The main drawbacks of TWs are i) the massive structure, ii) poor insulation, and iii) unbalanced performance for winter and summer (Hu, He, Ji, & Zhang, 2017). A lightweight, ventilated TW element (Lohmann & Santos, 2020) showed up to 27% savings on heating energy demand; summer conditions were not considered.

A thermal simulation model of the SEBF, including an approximation of vertical heat flows between the opaque and transparent areas, has been developed in Modelica. Modelica is an object orientated, equation-based language that can describe physical systems in various domains (Wetter, 2009). It supports transient thermal modelling and allows it to be combined with a customised control strategy for seasonal adaptive solar gain management. The model was validated against measurements on a test cell installation (Wüest, Grobe, & Luible, 2020).

The SEBF aims to turn the fundamental overheating susceptibility of DSFs (Manz & Frank, 2005; Balocco, 2002) into a means to improve the energy balance of buildings without active heat exchange. It aims to passively reduce heat losses in winter, and to control solar heat gains in summer. Preliminary studies (Wüest & Luible, 2018; Wüest & Luible, 2019) confirmed the fundamental design of the SEBF, and demonstrated the suitability of concrete and water as materials for the thermal storage. Nevertheless, both materials are difficult to integrate into lightweight façades. Concrete has a high dead load. Water implies the risk of leakage and freezing.

Latent heat storage techniques lend themselves as an alternative to these problematic materials (Biswas, 2016; Vukadinović, Radosavljević, & Đorđević, 2020). This research compares the performance of a SEBF element with thermal storage employing either water, concrete, or a set of Phase Change Materials (PCMs) by studying annual simulations under identical conditions.

2 MODEL DEVELOPMENT

For this study, the storage tank, made of a high absorbing aluminium tank within the DSF cavity, was simulated with different materials (gelled water, concrete, and two PCMs). In line with previous studies, all simulations were conducted in the Modelica modelling environment and were performed at intervals of one minute.

2.1 THE SOLAR ENERGY BALANCED FAÇADE

One-dimensional heat transfer elements from the Modelica standard library, e.g. Modelica. Thermal package, and its HeatTransfer sub-package were employed The SEBF was modelled as two one-dimensional heat flows through its transparent (A) and opaque (B) areas. These fluxes were coupled via a vertical heat exchange element (C1) within the air cavity (see Fig. 1). This approach has been validated experimentally (Wüest, Grobe, & Luible, 2020)

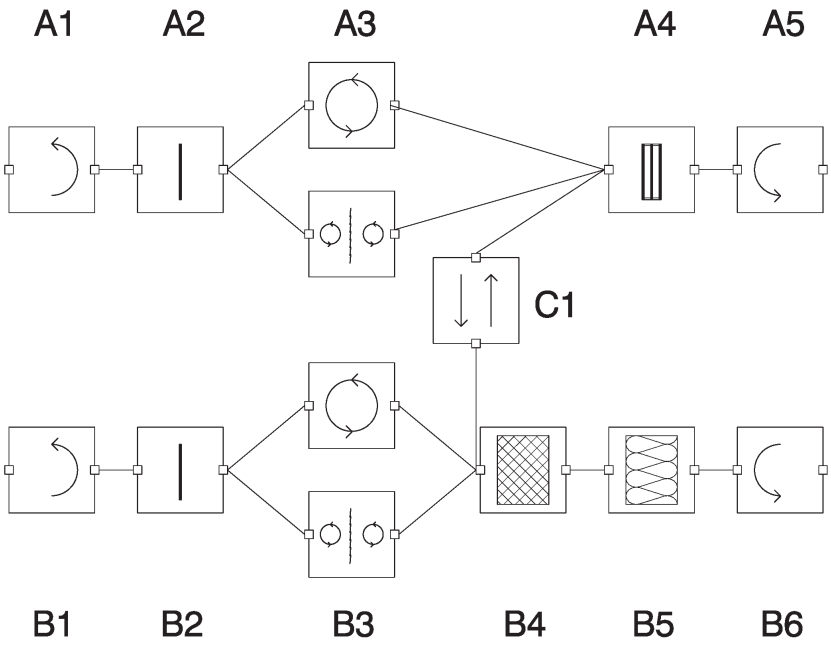

FIG. 1 Modelica model scheme for the four main components of the SEBF system

The modelling of convective heat flows on surfaces (external and internal) and through cavities was based on EN 15099. To simulate unsteady (transient) heat transfer, material layers were divided into *n* equidistant conductors, and *n+1* masses. Each conductor represents *1/n* of the layer thickness. The *n+1* masses represent the surfaces with two times *1/(2n)* of the total material layer mass and *n-1* times core masses of *1/n* of total material layer mass between the conductors (Wüest & Luible, 2019). This approach was applied with $n = 6$ to model the stack of storage materials and insulation forming the parapet. Glass panes and venetian blinds were simplified with $n = 2$ and only one centred mass. Air gap models A3 and B3 stand for the two different states without and with shading. The corresponding heat fluxes were modelled by one in the unshaded, and two convective and radiative conduction elements in the shaded case (acc. ISO 15099 section 8.3.2.2 and 8.4.3.1).

The elements in Fig. 1 are: external Solar Heat Transfer Coefficient (SHTC, A1 and B1), external glass pane (A2, B2), air gap with shading (A3 and B3 independent from each other), Triple Glazing Unit (TGU, A4), storage mass (B4), insulation (B5), internal SHTC (A5, B6), and vertical bi-directional heat flow element (C1).

2.2 HEAT CAPACITY OF PHASE CHANGE MATERIALS (PCMS)

Modelling PCMs in building simulation is challenging. The Modelica standard library is not designed for dynamic heat flow elements. Consequently, modelling heat transfer through PCMs with its irregularity (reflected by the heat storage capacity parameter), meant that the standard mass element had to be modified. The varying enthalpy due to the phase transition is described by a continuous temperature-dependent function (Halimov, Lauster, & Müller, 2019). For this research, the heat capacity during the melting and freezing process was approximated by a standard distribution. It was centred at the melting point $\mu = T_{melt}$. The standard variation σ was set to 1/6 of the melting range ΔT_{melt} (to include 99.73% of latent capacity within the melting range ΔT_{melt}). Its integral was scaled by the latent heat storage capacity (c_{lat}). Adding the sensible specific heat capacity (c_{sens}) leads to the dependent heat storage capacity ($c_{(T)}$) as described in Formula 1.

$$c_{(T)} = c_{sens} + c_{lat} \cdot \frac{1}{\sqrt{2 \cdot \pi \cdot \left(\frac{\Delta T_{melt}}{6}\right)^2}} \cdot e^{-\frac{(T - T_{melt})^2}{2 \cdot \left(\frac{\Delta T_{melt}}{6}\right)^2}} \qquad (1)$$

From the innumerable variants of PCMs, two exemplary storage materials from Rubitherm were used: high density salt-water PCM (SP29Eu) and organic PCM (RT25HC) as shown in Table 1. Fig. 2a illustrates the temperature dependent heat storage capacities ($c_{(T)}$), and Fig. 2 b and c the heat storages per kg and L respectively. It is evident that the two PCMs differ mostly by density, which accounts for the greater heat capacity per volume of SP29Eu.

In this research, only the effects of latent heat storage of PCMs were taken into account.
The influence of varying heat conductivities in solid and liquid states, as well as volume effects, were neglected. The thermal conductivity within the storage material layer is of minor influence and would lead to extended simulation time. A refined model taking account of varying heat conductivity could be realised in parallel to the described model.

TABLE 1 Exemplary PCMs evaluated in this research, source: https://www.rubitherm.eu/en/productCategories.html

PCM ID	PCM	MELTING POINT T_{MELT} [°C]	MELTING RANGE ΔT_{MELT} [K]	SENSIBLE SPECIFIC HEAT CAPACITY C_{SENS} [KJKG^{-1}K^{-1}]	LATENT HEAT STORAGE CAPACITY C_{LAT} [KJKG^{-1}]	DENSITY (SOLID) ρ [KGM^{-3}]
$PCM_{A(30/3)}$	SP29Eu	30	3	2'000	170'000	1525
$PCM_{B(25/5)}$	RT25HC	25	5	2'000	200'000	825

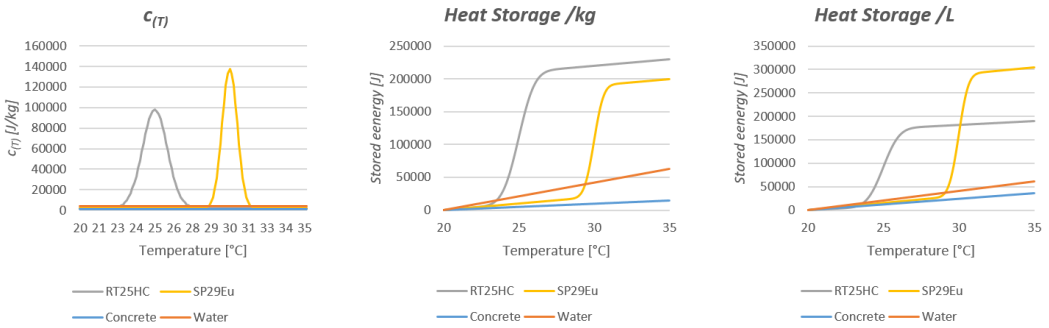

FIG. 2 Sensible and latent heat storage of PCM, concrete and water according Table 1 as a) function of temperature according to Formula 1, b) heat storage per kg, and c) heat storage per litre

3 EXPERIMENT

3.1 CONFIGURATION OF THE SOLAR ENERGY BALANCED FAÇADE AND EVALUATED STORAGE MATERIALS

The simulations only consider one SEBF element, 1.35 m x 2.9 m. The SEBF was configured so that its external layer is an 8 mm thick single pane of glazing (τ = 0.823, ρ = 0.076). The inner layer is horizontally divided into a parapet area of 1.5 m^2, and a transparent area covered by the TGU of 1.9 m^2. The depth of the cavity was set to about 150 mm in front of the TGU, and 100 mm in front of the storage. The shading was implemented by means of highly reflective Venetian blinds (ρ = 0.75).

The thermal storage tank consists of two 3 mm aluminium sheets with 20 mm or 40 mm of filling material (Table 2). The external surface of the tank has low reflectance and is highly absorbent (ρ = 0.25). The properties of the evaluated PCMs (PCM_A and PCM_B) were derived from the products reported in Table 1. They differ in terms of density, conductivity, and latent heat capacity.

TABLE 2 Relevant properties of the evaluated storage materials

MATERIAL	THICKNESS T [MM]	DENSITY ρ [KGM^{-3}]	CONDUCTIVITY Λ [$WM^{-1}K^{-1}$]	SPECIFIC HEAT CAPACITY C_{SENS} [JKG-1K-1]	LATENT HEAT CAPACITY C_{LAT} [JKG-1]	THERMAL EFFUSIVITY B [$JK^{-1}M^{-2}S^{-1/2}$]
Water Gel	20 /40	981	0.35	4'183	-	1198
Air	20 /40	Var.	Var.	-	-	-
Concrete	20 /40	2400	2.1	1'000	-	2245
PCM A	20 /40	1525	0.5	2'000	170'000	1235
PCM B	20 /40	825	0.2	2'000	200'000	575

3.2 VARIATIONS OF STORAGE MATERIALS

The selection of the PCMs is challenging due to the wide range of properties of available materials and products, which by no means is represented by the selection of the two PCMs (Table 1). The selection of the two PCMs is rather regarded as an example by which to evaluate the effect two different types—organic and high density—on the performance of the SEBF's thermal storage.

The effectivity of PCMs is mainly defined by their melting temperatures. To activate the latent heat storage, variants of the PCM types were chosen with melting points low enough to be reached on cold and sunny winter days, but high enough to be discharged on summer nights. In the simulation experiment, each of PCM_A and PCM_B was evaluated assuming three different melting points: 25°C, 30°C, and 35°C.

In the following passages, PCM types (A or B) and their variants (defined by T_{melt} and ΔT_{melt}) are indicated as subscripts. A PCM of type A with T_{melt} = 35°C and ΔT_{melt} = 5 K would therefore be referred to as $PCM_{A(35/5)}$.

The simulations assume an initial maximum depth of the storage material of 40 mm. This is motivated by the identical geometric configuration of the SEBF evaluated in a precedent study, the results of which shall be compared to Wüest, Grobe, and Luible (2020). In addition, the effect of decreasing the thickness by of 50% to = 20 mm was analysed.

Water and concrete were modelled as reported by Table 2. In parallel with the previous research, all results were compared to the case of an empty storage tank (material "air"). This allows the effects of the thermal mass of the storage to be isolated from those of other solar-optical mechanisms.

3.2.1 Shading Control

To make use of solar gains in cold periods but prevent overheating during warmer periods, a customised control of the shading devices in the transparent and opaque zones was employed. The control enters three predefined modes based on the mean average external temperature over the last 24 hours T_{24} (Wüest, Grobe, & Luible, 2020). If T_{24} is lower than 12°C, the system is in heating mode and maximises solar gains. If T_{24} is higher than 15°C, the SEBF is in cooling mode and minimises gains. The range between 12° and 15° activates 'free floating' mode, avoiding gains through the storage, and moderating direct gains through the TGU. The set points of the modes are listed in Table 3. In all three modes, night-time losses are controlled by application of a threshold of 25 W/m2 to monitored global vertical irradiance E_v.

TABLE 3 Global irradiance set points for shading control

RESPONSE	HEATING MODE $T_{24} \leq 12°C$	FREE FLOAT MODE $12°C < T_{24} < 15°C$	COOLING MODE $15°C \leq T_{24}$
Close shading of TGU	if $E_v > 350$ W/m²	if $E_v > 350$ W/m²	if $E_v > 150$ W/m²
Close shading of TGU at night	always	always	never
Close shading of storage	if $E_v < 25$ W/m²	if $E_v > 25$ W/m²	if $E_v > 25$ W/m²
Close shading of storage at night	always	never	never

3.3 BOUNDARY CONDITIONS

In all simulations, internal air temperature was set to 22°C. Influences of occupancy were not considered. The outdoor conditions were given by a standard design year for Zürich (CH) on an hourly basis from Meteonorm (Meteotest AG, 2018). All parameters, such as temperature, wind speed, façade irradiance, and sun position were interpolated linearly from hourly values.

3.4 EVALUATION VARIABLES

The effect of varying storage materials was evaluated by four variables that were solved by the simulation:

- the maximum surface temperature of the storage tank,
- the energy balance of the SEBF element for each season,
- short-term effects such over the course of the day, and
- the dead load introduced into the façade by the storage material.

The maximum surface temperature of the storage tank was expected to be the warmest point within the SEBF element. Because of its non-ventilated DSF structure, the façade tends to overheat (Manz & Frank, 2005). Therefore, the maximum temperature within the element acts as an indicator for thermal loads on the SEBF's component. High temperatures could, for example, accelerate ageing processes or lead to fogging (outgazing of plasticisers and condensation on the glass surface).

Effects on the energy balance, as the primary design target of the SEBFs, were evaluated as the key output of the simulation. Therefore, the heat flow at the inner façade surface is regarded to evaluate the needed heating or cooling demand in the interior. To reduce complexity, the thermal balance of an SEBF element was evaluated seasonally for winter (January, February, December), spring (March, April, May), summer (June, July, August), and autumn (September, October, November). To evaluate the intended delay of passive solar gains, as the secondary design target, one winter and one summer day were analysed in detail.

The dead load imposed by building materials significantly affects the structural design of curtain walls. Traditionally, the weight of glass accounts for the largest proportion of the dead load on façade elements. A typical TGU for façade applications consists of about 21 mm glass (comprising three panes of 8 mm, 5 mm and 8 mm), corresponding to a dead load of 57 kg/m^2. This is the reference for the storage tank, where 29 kg/m^2 is contributed by the containing aluminium sheets (~10 mm) and insulation (70 mm) alone.

4 RESULTS

4.1 TEMPERATURES

Table 3 shows that the shading control is effective in that the storage tank only receives solar irradiance when the external 24-hour mean temperature T_{24} is below 12°. Since this effectively blocks irradiance on hot days in summer, the maximum surface temperatures of the storage occur

only from September until April. In summertime (June – August), they rarely surpass 40°C for the 40 mm tank, while the storage of reduced thickness of 20 mm reaches 47°C, and the empty (air-filled) tank 53°C. Fig 3 distils these findings by showing only the daily maximum temperatures T_{max} on the storage tank in its 40 mm, 20 mm, and air configurations.

The maximum temperatures for the entire year are summarised in Fig. 4. All configurations, except of air, reach higher temperatures when the thickness of storage material is reduced. The air element reaches the highest temperatures, up to 88°C, whereas the 40 mm water element, as proposed in the initial design of the SEBF, is significantly cooler at approximately 63°C. The variants of PCM_B with a thickness of 40 mm achieve similar results to 40 mm of water. With PCM_A, the maximum temperatures are significantly lower. Even the 20 mm configurations of $PCM_{A(30/3)}$ and $PCM_{A(35/3)}$ are at the same level as a water-filled tank of twice the volume.

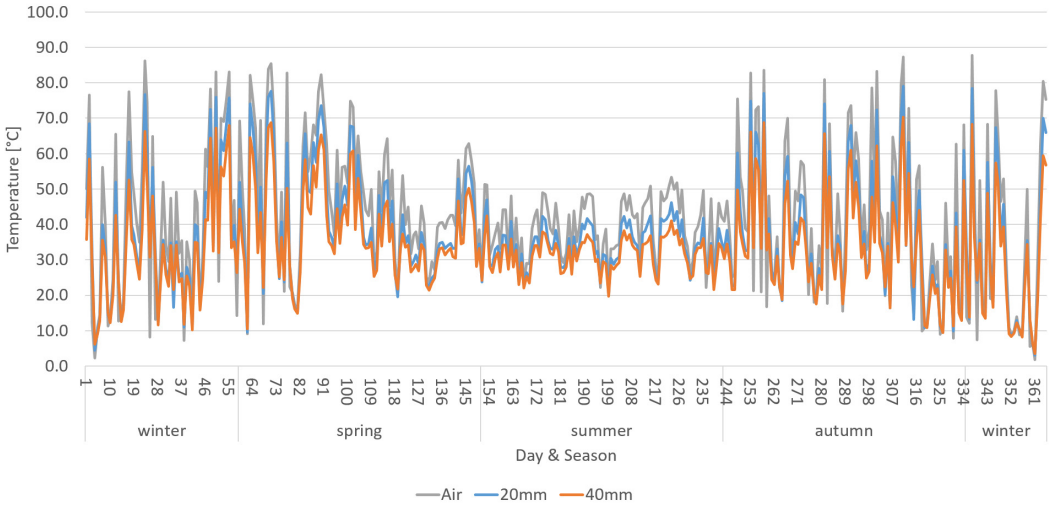

FIG. 3 Maximum tank surface temperature Tmax of 40 mm, 20 mm and air configurations, in °C

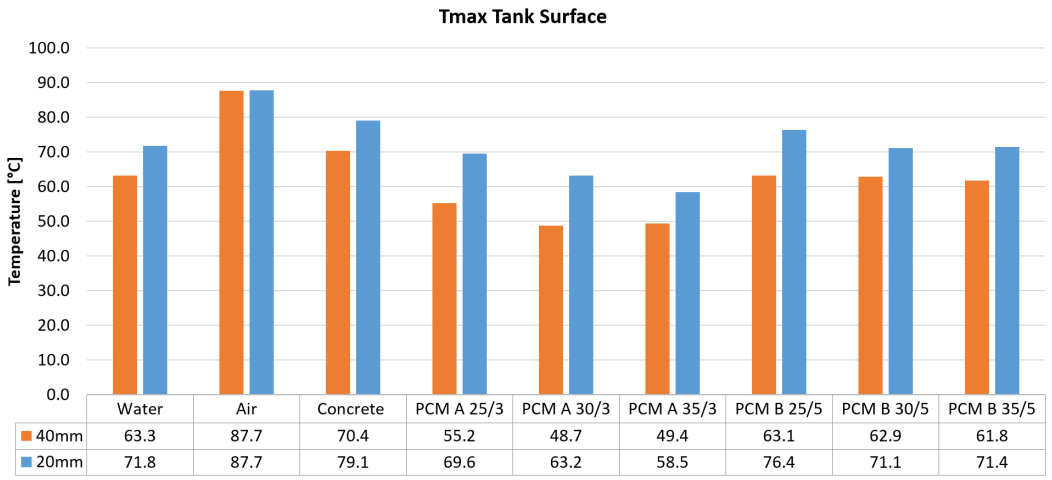

	Water	Air	Concrete	PCM A 25/3	PCM A 30/3	PCM A 35/3	PCM B 25/5	PCM B 30/5	PCM B 35/5
40mm	63.3	87.7	70.4	55.2	48.7	49.4	63.1	62.9	61.8
20mm	71.8	87.7	79.1	69.6	63.2	58.5	76.4	71.1	71.4

FIG. 4 Maximum annual tank surface Temperatures Tmax for all storage material configurations, in °C

4.2 ENERGY BALANCE FOR EACH SEASON

The energy balance at the internal façade surface for each season due to heat conduction for all storage variants is summarised in Table 4. In addition, the direct solar heat gains are reported, which are identical for all elements. All configurations achieve similar results, especially in winter and summer. Higher differences occur at intermediate climate conditions in spring and autumn.

TABLE 4 Energy balance for each element and season in [kWh]

		WATER	AIR	CON-CRETE	PCM A 25/3	PCM A 30/3	PCM A 35/3	PCM B 25/5	PCM B 30/5	PCM B 35/5	DIR. SOL. GAIN
40 mm	**Winter**	-29.0	-32.2	-29.6	-29.3	-29.1	-28.6	-30.3	-30.1	-30.2	28.8
	Spring	5.8	2.5	5.3	5.63	6.1	6.7	5.00	5.2	5.2	52.9
	Summer	13.6	15.5	13.6	13.0	13.4	13.6	13.4	13.6	14.0	35.8
	Autumn	-4.1	-5.6	-4.4	-4.5	-4.0	-3.9	-4.9	-5.02	-4.7	37.7
20 mm	**Winter**	-30.2	-32.3	-31.5	-29.4	-29.8	-29.20	-30.6	-30.8	-30.7	
	Spring	4.9	2.3	3.7	5.7	6.1	6.27	5.2	5.0	4.8	
	Summer	13.9	15.4	14.3	13.0	13.5	13.9	13.5	13.7	14.2	
	Autumn	-4.7	-5.8	-5.4	-4.8	-4.3	-4.2	-5.01	-5.2	-5.0	

Table 5 shows the percentage deviation relative to the 40 mm water tank for winter and summer periods. As reported by Table 4, only the empty tank leads to significantly higher heat losses and gains (11% to 14%).

TABLE 5 Energy balance for each element an season in [kWh]

		WATER	AIR	CON-CRETE	PCM A 25/3	PCM A 30/3	PCM A 35/3	PCM B 25/5	PCM B 30/5	PCM B 35/5
40 mm	**Winter**	0%	11%	2%	1%	0%	-1%	4%	4%	4%
	Summer	0%	14%	0%	-4%	-2%	0%	-2%	0%	3%
20 mm	**Winter**	4%	11%	9%	1%	3%	1%	5%	6%	6%
	Summer	2%	13%	5%	-5%	-1%	2%	-1%	0%	4%

4.3 SHORT-TERM ENERGY BALANCE

The short-term energy balance is presented for two sample days each for both winter (Fig. 7) and summer (Fig. 8). The corresponding exterior conditions are illustrated by Fig. 5 and Fig. 6. The two days in February represent the coldest two-day period (nights below -7°C), whereas the two days in July represent the warmest two-day period (peak 32.7°C).

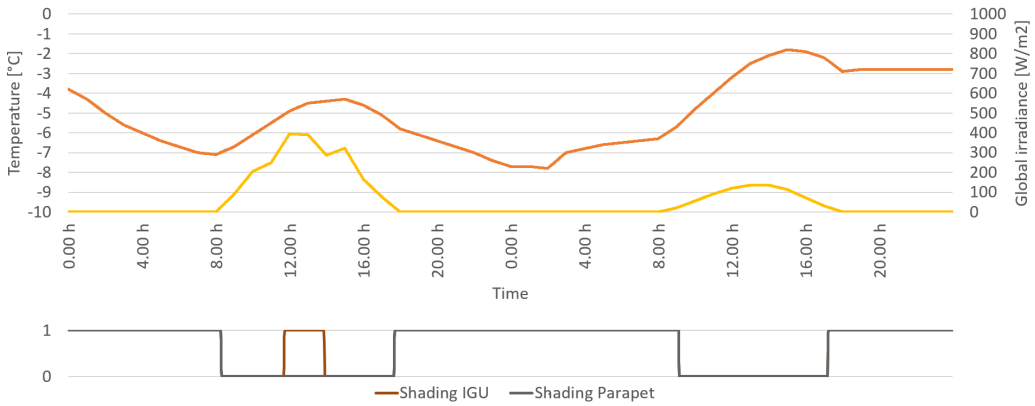

FIG. 5 External conditions (air temperature, solar irradiance façade) 9th – 10th February according Meteonorm

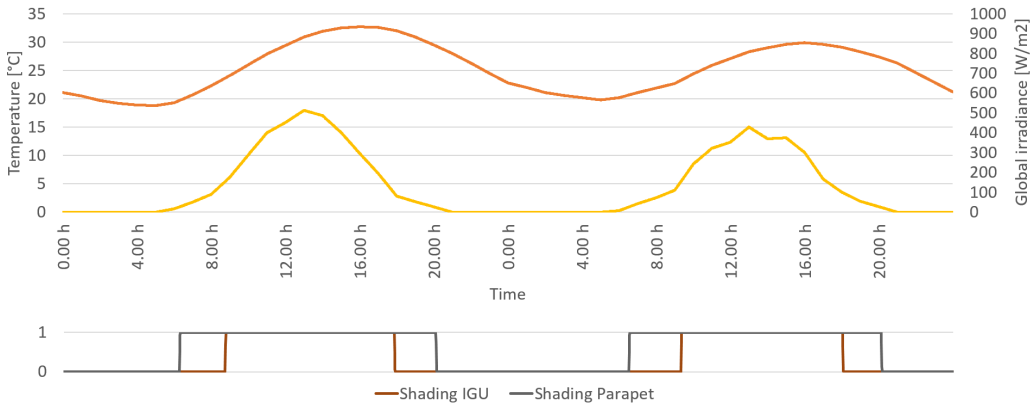

FIG. 6 External conditions (air temperature, solar irradiance façade) 24th – 25th July according Meteonorm

Both Fig. 7 and Fig. 8 confirm the short-term behaviours of what Table 4 and Table 5 indicate as seasonal effects: all storage variants act very similarly. Heat is mostly stored and released within 24 hours. Therefore, only 40 mm water and 40 mm air variants were highlighted within the figures. A first analysis of those graphs reveals the following main findings:

- All parapet heat flows are slightly undulated and close to zero,
- all TGU heat flows are extremely volatile, because they react immediately to solar irradiance,
- higher solar irradiance increases the differences in heat flows,
- due to the low temperature and solar irradiance in winter (9th -10th February), the storage is almost ineffective, leading to nearly identical heat flows through all configurations, and
- the effects of PCMs are reflected by plateaus of constant heat flow in summer at values decreasing with melting temperature, e.g. 2 W, 4 W, and 7 W for melting temperatures of 25°C, 30°C, and 35°C => 7 W respectively.

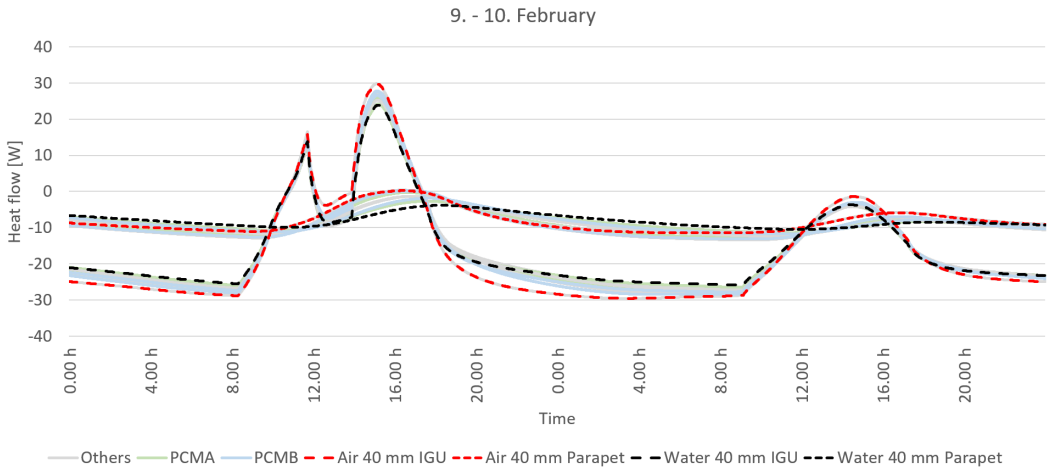

FIG. 7 Two-day period winter (9th – 10th February) heat flows

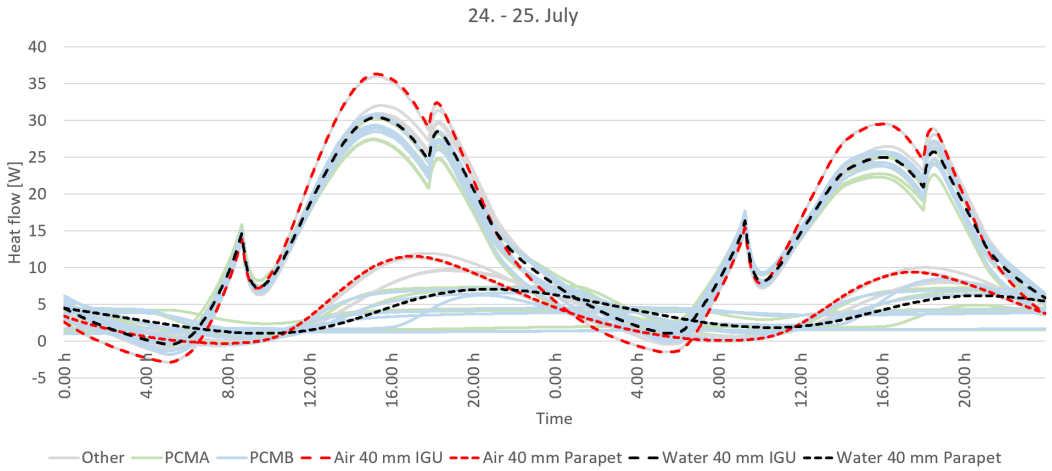

FIG. 8 Two-day period summer (24th – 25th July) heat flows

4.4 DEAD LOAD

The effect of the evaluated storage materials on the dead load of the SEBF is evaluated in comparison to a transparent parapet comprising a TGU with a typical glass mass (21 mm) of 57 kg m^{-2}.
The additional mass of 29 kg m^{-2} is taken into account for the supporting structure required for the storage tank (aluminium and insulation). Table 6 reports the dead load per unit area corresponding to the evaluated storage materials compared to a TGU.

TABLE 6 Storage materials dead load

MATERIAL	THICKNESS T [MM]	DENSITY ρ [KGM^{-3}]	MASS M [KGM^{-2}]	ADDITIONAL TANK MASS M_{TANK} [KGM^{-2}]	TOTAL MASS M_{TOT} [KGM^{-2}]	TO REFERENCE TGU (57 KGM^{-2}) [KGM^{-2}]
Water Gel	20	981	19.6	29	48.6	-8.4
	40	981	39.2	29	68.2	+11.2
Concrete	20	2400	48.0	29	77	+20
	40	2400	96.0	29	125	+68
PCM A	20	1525	30.5	29	59.5	+2.5
	40	1525	61	29	90	+33
PCM B	20	825	16.5	29	45.5	-11.5
	40	825	33.0	29	62	+5

5 CONCLUSIONS

As expected, with increasing thermal mass the tank surface temperature and therefore the overheating risk decrease. The tested high density PCM (PCM_A) limited the maximum temperatures on the storage tank, indicating the potential to limit the risk of overheating and thermal stress on façade components. Concrete and PCM_B had adverse effects. With all evaluated storage materials, surface temperatures covered a wide range from approximately 0°C to 70°C. Under such extreme fluctuations, the beneficial effects of the latent heat storage capacity of PCMs are not fully leveraged due to its low sensitivity. It has to be noted that some PCMs might become in stable at the high temperatures that can occur within a non-ventilated DSF, e.g. up to 76.4°C in the studied configurations.

The differences in overserved effects on seasonal and short-term energy balances by the tested storage materials were low. This holds true even with significantly different sensitive and latent heat storage capacities. This can be explained by effects of the thermal effusivity *b*, which is a measure of a material's ability to exchange and store thermal energy. Regarding the formula of thermal effusivity , a high influence of thermal conductivity appears. Compared to water gel, concrete, for example, has a 42% lower volumetric heat capacity (ρ*c), but almost twice its thermal effusivity. Consequently, concrete has a lower heat capacity but higher exploitation. For PCM_A and PCM_B, effusivity differs by a factor of approximately 2 due to their significantly different conductivities (see Table 2).

The particularly high dead load introduced into the SEBF by concrete as a storage material based on high density is problematic. This drove the motivation to rely on water, with its outstanding specific heat capacity, in the first implementations of the SEBF, although the integration of a liquid into a façade element was expected to be challenging. The dead load introduced by PCM_A due to its high density seems to be a problem at first glance. On further observation, Table 6 shows that 20 mm PCM_A is competitive against 40 mm water gel and, therefore, a good option to reduce weight and enhance thermal performance. The dead load of PCM_B in 40 mm is not problematic, but, due to its low thermal effusivity *b*, the volume is poorly exploited.

In this comparison, the PCM_A of 20 mm shows the highest potential for the application in terms of dead load and thermal effects. To sum up, the application of PCM as thermal storage material within non-ventilated DSFs is possible and justified. Nevertheless, the results of this research indicate that the main benefit of PCMs is not their effects on energy balance, but rather space and weight saving within the construction when compared to other storage materials. The choice should be carried out carefully and not just be based on sensitive and latent storage capacity. Density and conductivity (thermal effusivity) could decide between success and failure in a particular application. As mentioned, PCM_A seems promising for this application. However, further investigation on the right combination of its properties (λ, ρ, c_{sens}, c_{lat}) for a DSF storage application could further improve thermal and structural aspects.

For future development of the SEBF or similar elements, two conclusions are made: a) PCM could enhance thermal performance, but non-PCM materials could also contribute to improved energy balance; and b) the choice of a suitable PCM needs an in-depth evaluation to find the right material. Furthermore, besides the criteria in this work, other criteria as processability, availability, durability, price and so on should be considered.

Acknowledgements

The authors gratefully acknowledge the funding provided by the Swiss National Science Foundation (SNF), Grant No. IZCNZ0-174562).

References

Balocco, C. (2002). A simple model to study ventilated façades energy performance. *Energy and Buildings, 34*, pp. 469-475. https://doi.org/10.1016/S0378-7788(01)00130-X

Biswas, D. (2016). Nano-based phase change materials for building energy efficiency*. *Start-Up Creation*, pp. 183-211. https://doi.org/10.1016/B978-0-08-100546-0.00009-1

Halimov, A., Lauster, M., & Müller, D. (2019). Validation and integration of a latent heat storage model into building envelopes of a high-order building model for Modelica library AixLib. *Energy and Buildings, 202,* p. 109336. https://doi.org/10.1016/j.enbuild.2019.109336.

Hu, Z., He, W., Ji, J., & Zhang, S. (2017). A review on the application of Trombe wall system in buildings. *Renewable and Sustainable Energy Reviews,* 70, pp. 976-987. https://doi.org/10.1016/j.rser.2016.12.003

ISO 15099. (2003). *Thermal performance of windows, doors and shading devices - detailed calculations.* Geneva: ISO copyright office.

Lohmann, V., & Santos, P. (2020). Trombe wall thermal behaviour and energy efficiency of a light steel frame compartment: Experimental and numerical assessments. *Energies,* 13, p. 2744. https://www.mdpi.com/1996-1073/13/11/2744

Manz, H., & Frank, T. (2005). Thermal simulation of buildings with double-skin façades. *Energy and Buildings, 37*, pp. 1114-1121. https://doi.org/10.1016/j.enbuild.2005.06.014

Meteotest AG. (2018). *Meteonorm V7.3.3*. Bern Switzerland.

Quesada, G., Rousse, D., Dutil, Y., Badache, M., & Hallé, S. (2012). A comprehensive review of solar façades. Opaque solar façades. *Reviews, Renewable and Sustainable Energy,* 16, pp. 2820-2832. https://doi.org/10.1016/j.rser.2012.01.078

Vukadinović, A., Radosavljević, J., & Đorđević, A. (2020). Energy performance impact of using phase-change materials in thermal storage walls of detached residential buildings with a sunspace. *Solar Energy,* 206, pp. 228-244. https://doi.org/10.1016/j.solener.2020.06.008

Wetter, M. (2009). Modelica-based modelling and simulation to support research and development in building energy and control systems. *Journal of Building Performance Simulation,* pp. 143-161. https://doi.org/10.1080/19401490902818259

Wüest, T., & Luible A. (2019). Trombe curtain wall façade. *PowerSkin Conference Proceedings,* p. 313. Retrieved from https://books.bk.tudelft.nl/index.php/press/catalog/view/isbn_9789463661256/786/679-3

Wüest, T., & Luible, A. (2018). Solar Energy Balanced Façade. Façade 2018 - Adaptive! *Proceedings of the COST Action TU1403 Adaptive Façades Network Final Conference,* pp. 183-194.

Wüest, T., Grobe, L. O., & Luible, A. (2020). An Innovative Façade Element with Controlled Solar-Thermal Collector and Storage. *Sustainability,* 12, p. 5281. https://doi.org/10.3390/su12135281

Zhang, L., Hou, Y., Lui, Z., Du, J., Xu, L., Zhang, G., & Shi, L. (2020). Trombe wall for a residential building in Sichuan-Tibet alpine valley – A case study. *Renewable Energy,* 156, pp. 31-46. https://doi.org/10.1016/j.renene.2020.04.067